SELECT CO2

SELECTIVE ELECTROCHEMICAL REDUCTION OF CO2 TO HIGH VALUE CHEMICALS

Grant agreement no.: 851441
Start date: 01.01.2020 – **Duration**: 36 months
Project Coordinator: Dr. Brian Seger - DTU

DELIVERABLE REPORT

D3.2– REPORT ON SNIFFER CHIP DISCOVERIES RELATING TO ETHANOL/ETHYLENE BRANCHING MECHANISM	
Due Date	31/05/2021
Author (s)	Yu Qiao
Workpackage	3
Workpackage Leader	Brian Seger
Lead Beneficiary	DTU
Date released by WP leader	28/5/2021
Date released by Coordinator	28/5/2021

DISSEMINATION LEVEL		
PU	*Public*	*X*
PP	*Restricted to other programme participants (including the Commission Services)*	
RE	*Restricted to a group specified by the consortium (including the Commission Services)*	
CO	*Confidential, only for members of the consortium (including the Commission Services)*	

NATURE OF THE DELIVERABLE		
R	*Report*	*X*
P	*Prototype*	
D	*Demonstrator*	
O	*Other*	

SUMMARY	
Keywords	*Electrochemical CO/CO$_2$ reduction, KHCO$_3$ dissociation, Cu/Au tandem catalysts, ethylene/ethanol bifurcation, faradaic efficiency, EC-MS, selective ionization, CO production, local pH*
Abstract	*Ethanol/ethylene bifurcation in electrochemical CO$_2$ reduction (ECO$_2$R) on Cu has been a challenging project due to its low selectivity towards C$_2$ products. Recent studies have found that Au sites in CuAu tandem catalysts could create a high local CO concentration at the vicinity of the Cu sites, where C-C coupling happens subsequently. However, the interaction been Cu and Au still remains obscure. In this report, we examined the electrochemical CO2/CO reduction activities on Cu and Au separately in order to provide preliminary possibilities for future studies on the Cu-Au interplay. Taking advantage of the highly sensitive EC-MS setup with its Sniffer Chip technology, early onset of C$_2$ products was observed on both Cu and Au electrodes. Selective ionization was applied to ECO$_2$R on Au to extract the contribution of CO$_2$ fragmentation from the "real" CO in m/z 28 signals. Electrocatalysis on roughened surfaces revealed a remarkably promoted CO production while a significantly suppressed HER, which is distinct from previous findings. It was preliminarily explained as a combined influence from the local pH and electric field. Surface roughness and overpotential may also have an impact on the reaction mechanism, which will be further investigated in the future. Dissociation of Ar-saturated KHCO$_3$ under ECO$_2$R conditions provided direct evidence on the internally produced CO$_2$, which was reduced to CO subsequently, even in the absence of an external CO$_2$ supply. The obtained results provide insightful information on the potential interplay between CuAu in tandem catalysis, as well as the electrode-electrolyte interactions on the ECO$_2$R/ECOR reaction mechanism. However, The current results are mostly based on qualitative evaluation. More deliberated quantitative analysis will be the main focus in the future. A detailed future plan was stated in Section 4.*
Public abstract for confidential deliverables	

REVISIONS			
Version	**Date**	**Changed by**	**Comments**
0.1	26/05/2021	Yu Qiao	

REPORT ON SNIFFER CHIP DISCOVERIES RELATING TO ETHANOL/ETHYLENE BRANCHING MECHANISM

CONTENTS

SELECTCO2 Deliverable Report D.3.2 – Report on Sniffer Chip discoveries relating to ethanol/ethylene branching mechanism - 28/05/2021 – Version 1.0

3

1. INTRODUCTION

Electrochemical CO_2 reduction (ECO_2R) converts greenhouse gas CO_2 into valuable fuels and chemicals, and thus helps with closing the anthropogenic carbon cycle. Currently, Cu is the only known material being capable of producing a variety of hydrocarbons and alcohols, while the poor selectivity limits its further use [1]. Compared to C_1 products (CO, CH_4, and formate), C_2 products (e.g., C_2H_4, C_2H_6, and ethanol) have higher energy densities and larger economic values [2], and therefore attracts more attention. While Cu is sluggish in converting CO_2 to CO, it is much more active in further converting CO to more highly reduced species. However, due to the low solubility of CO in water (~1 mM at 1 atm and 25°C) [3], deliberate strategies to promote CO availability on catalyst surfaces are sought after. To this end, tandem catalysts combining Cu and a CO-selective metal (Ag, Au, and Zn) have proven their superiority. Among the CO-selective metals, Au is generally the most active ECO_2R catalyst owing to its intrinsically stronger binding of *C-species [4]. In a tandem mechanism, Au produces a large amount of CO, which then "spillover" to the neighboring Cu catalysts, leading to a locally nearly saturated [5] or even over-saturated [6] CO concentration at the adjacent Cu active sites. Since *CO and *H compete for the same adsorption sites on Cu under ECO_2R conditions [7], the high CO coverage not only facilitates C-C coupling, but suppresses hydrogen adsorption and thus the competing hydrogen evolution reaction (HER) as well [5]–[8]. For example, by tuning the exposed Cu-Au interface area on an Au substrate lithographically patterned with Cu dots/lines, Lum and Ager increased the oxygenate to ethylene ratio in ECO_2R compared to the case when only Cu was involved [6]. Morales-Guio et al. promoted the selectivity of C_2 to C_1 products to over two orders of magnitude by depositing Au nanoparticles on polycrystalline Cu surface [5].

Among the various C_{2+} products formed on Cu, ethanol (EtOH) has the highest energy density (26.8 MJ/kg) and is also a widely used intermediate in chemical synthesis [9], [10]. However, its faradaic efficiency is usually lower compared to ethylene (C_2H_4) in ECO_2R, which is believed to undergo a competing pathway to ethanol production [9], [11]. It has been found that introducing Au atoms into Cu lattice could shift the product distribution toward ethanol compared to ethylene [5], [7], [11], [12]. Jia et al. obtained 28% of alcohol (methanol and ethanol) on the prepared nanostructured Cu-Au, which was 3 times that on pure nanostructured Cu and pure Au nanoparticles did not produce ethanol. Although these results suggest that the interaction between Cu and Au contributes to the enhanced conversion of CO_2 to alcohols, the detailed formation mechanisms of alcohols remain obscure. [12] Interestingly, Morales-Guio noticed a 1.3~2.0 ratio of alcohol/hydrocarbon at low overpotential (-0.7~-0.9V vs. RHE), while it significantly decreased as the potential became more negative. The reason was speculated as a combined effect of i) a lower binding strength for CO due to the relatively positive bias, ii) a weaker proton/water reduction at low overpotentials, and iii) the high local CO concentration attributed to the tandem catalysis mechanism between Au and Cu. More explicit demonstration merits further discussion. [5] Another study on Cu_3Au alloy nanoparticle embedded Cu submicrocone arrays reached a 29±4% Faradaic efficiency of EtOH, while C_2H_4 formation was attenuated (16±4%). Density functional theory (DFT) calculations showed that the d-band center of Cu moved close to its Fermi level owing to the stretched lattice by introducing Au atoms. [11] According to the d-band model, an upshifted d-band center would strengthen the adsorbed intermediates [13]. As a result, the C-O bond in CH_2CHO* was weakened on Cu_3Au, leading to an increased EtOH production over C2H4. On the contrary, Liu et al. noticed the d-band center of Cu gradually shifted away from the Fermi level with Au atomic ratio increased, leading to a weakened binding energy of *CO [14]. Kim et al. reported a similar phenomenon and revealed that s electrons transferred from Cu to Au using photoemission spectroscopy (PES) [15]. However, it was also elucidated that a slight depletion of electron in Cu could enhance the binding of CO, which in turn facilitates C-C coupling [16].

The above contradictories demonstrate a yet-to-be-clarified mechanism of the interaction between Cu and Au in ECO$_2$R. In order to get more insights into the mechanisms, we will use an EC-MS system developed at DTU (**Error! Reference source not found.**), which allows real-time detection of reaction products and intermediates during electrochemical experiments via a quadrupole mass spectrometer (QMS). Being capable of resolving and quantifying submonolayer amounts of gaseous products on a scale of seconds as sub-turnover resolution with a 100% collection efficiency [17], the EC-MS system enables us to see the early onset of the products at low overpotentials during electrochemical measurements.

To this end, we will first investigate ECO$_2$R on Cu and Ag separately. ECOR on Cu will also be studied since CO$_2$ to CO has been found to be the RDS for C-C coupling and it is the first isolable product and intermediate of ECO$_2$R for further generating multi-carbon products; moreover, the pH of the electrolyte solution is independent of CO concentration [18]. Bimetallic catalysts of Cu and Au will be prepared subsequently via various methods, such as sputtering, lithography, electro-deposition, and galvanic exchange. By this means, different Cu/Au interfaces and hence interactions can be expected and further investigated.

This report will focus on ECO$_2$R and ECOR on pure Cu and Au electrodes at low overpotentials (< -0.8V). Considering that the ionization of CO$_2$ produces CO$^+$ fragments which interfere with the real CO signal in the QMS, selective ionization with a lower ionization energy was conducted to moderate CO$_2$ dissociation. Besides, KHCO$_3$ dissociation will also be investigated to get a better perception on the homogeneous equilibrium in the electrolyte. The interaction between Cu and Au will be studied in the future. Moreover, due to the limitation of the EC-MS system in probing liquid products, the current report will focus on gas-phase products, such as CO and C$_2$H$_4$. Future works involved with liquid product detection will be carried out on an H-type cell and high-pressure liquid chromatography (HPLC) or nuclear magnetic resonance (NMR).

The presented results in this report are based on filament currents directly acquired from the QMS. Due to technical issues on the current EC-MS setup, the experimental results in terms of Faradaic efficiency and partial current density were converted and compared qualitatively, while absolute values are unfortunately unavailable so far. An identical system will be swapped in June 2021, after which quantitative analysis will be applicable.

2. SCOPE

A pure Cu (metal trace >99.9999%) electrode was used for ECO$_2$R and ECOR in a stagnant thin layer electrochemistry cell (**Error! Reference source not found.**). Benefiting from the high time resolution and sensitivity, as well as its 100% gaseous product collection efficiency, we were able to observe relatively low onset potentials of C$_2$H$_4$ and CH$_4$ at -1.05 V and -1.20 V vs. the Standard Hydrogen Electrode (SHE), corresponding to -0.37 V and -0.52 V vs. the Reversible Hydrogen Electrode (RHE), respectively. The observed low onset potential verifies the capability of detecting a minute amount of the generated gaseous products using the EC-MS system.

Selective ionization was realized on the QMS by reducing the ionization energy of the filament and therefore mitigated the contribution of the CO$^+$ fragments from CO$_2$ dissociation in the mass 28 signal. The activities and selectivities of a pure Au (metal trace >99.999%) electrode with flat and roughened surfaces were measured and compared. The distinct performance on various surfaces and overpotentials implies possibly different mechanisms, while the highly sensitive EC-MS setup will give more insights in this regard.

The decomposition of the most commonly used $KHCO_3$ electrolyte was also studied by saturating with Ar. Results confirmed that CO_2 could be generated internally in the electrolyte due to the homogenous equilibrium among the buffering species, and produced CO even in the absence of an external CO_2 supply. These results give a better understanding on the influence of local pH. Considering that CO is one of the most important intermediates for C-C coupling in ECO_2R, these results will give better insights into understanding the interaction of buffering species in the electrolyte on the ECO_2R mechanisms.

This report will provide useful information on the interaction between Cu and Au in bimetallic catalysts for C-C coupling and ethanol production in ECO_2R. Furthermore, quantitative analysis on CO_2 consumption will be easily realized on the EC-MS setup, by combining selective ionization and $KHCO_3$ dissociation, and thus provide more insights into the electrode-electrolyte interaction in ECO_2R.

3. DISCUSSION

3.1 Experimental
Electrolyte Preparation
K_2CO_3 solutions were prepared by dissolving K_2CO_3 (99.995% trace metals basis, Aldrich) into MilliQ water (18.2 MΩ.cm @25°C, 2ppb TOC, Q-POD®). 0.1M $KHCO_3$ solution was prepared by purging CO_2 (N45, Air Liquide) into 0.05M K_2CO_3 solution for at least 30min, until pH~6.8. Metallic impurities in electrolytes were removed by chelating with Chelex® 100 (sodium form, 100-200 mesh particle size, Sigma-Aldrich) [19].

Electrode preparation
The gold (polycrystalline) and copper (polycrystalline) working electrodes were both purchased from Sigma-Aldrich. The exposed surfaces of the working electrodes were both 0.5cm in diameter. A gold film (0.5cm*0.5cm, 99.99%, Goodfellow) and Hg/Hg_2SO_4 (K_2SO_4 0.6 mol/l, B 3610+, VMR) were used as the counter and reference electrode, respectively.

The counter and reference electrodes were rinsed with MilliQ water before use. The copper working electrode was mechanically polished with MicroPolish™ Alumina (0.3μm, Buehller) on a MicroCloth polishing cloth (Buehler) and subsequently rinsed and sonicated with MilliQ water prior to use.

The gold working electrode was flame annealed (Proxxon) after polishing and washing as described above. The Au electrode right after annealing was marked as "pristine". Roughening of the Au electrode was conducted subsequently *in situ* by cycling at 1.05V and 2.75V vs. RHE (0.65V and 2.35V vs. SHE) for 1h, keeping at each potential for 2s. The electrode was then kept at -0.35V vs. RHE for 1h to reduce the Au oxide layer. After surface reduction was completed, the potential was changed back to the open circuit potential (E_{oc}) and kept there until the QMS signals of all analytes stabilize at their background levels, prior to initiating electrocatalysis at 0V vs. RHE.

Electrochemical setup
All experiments were carried out with a commercially available microchip-based EC–MS setup (SpectroInlets ApS, Denmark) with a stagnant thin-layer cell (**Error! Reference source not found.**). The counter and reference electrodes were inserted in a glass tube with a ceramic frit on the tip, respectively. The working volume is defined by the distance between the working electrode and the membrane chip, which is 100μm. A carrier gas is normally required to equilibrate the chip pressure with atmosphere. When the carrier gas also works as the reactant (e.g. CO_2 as the carrier gas for ECO_2R, and CO as the carrier gas for ECOR), it diffuses through the micro holes on the chip

to the working volume, where it has the chance to reach the working electrode and participate in the electrochemical reaction. Afterwards the excessive carrier gas and produced molecules desorb from the working electrode and diffuse through the membrane chip to the QMS. For more details regarding the design and working mechanism of the system please refer to [17].

It is worth noting that due to the high sensitivity and small reaction volume, when too much gas is produced in the system, the potentiostat is easily overloaded, which limits the overpotential below 1.0V in most cases (with the exact maximum potential a function of the current/produced gas). This issue will be described in more detail in each case below.

Electrochemical measurements

0.1M $KHCO_3$ and 0.1M K_2CO_3 electrolytes were used for ECO_2R and ECOR, respectively. Prior to each measurement, the electrolytes were purged with the carrier gas (i.e. CO_2, CO (HiQ, 4.7N), and He (6.0M, Air Liquide)) for at least 30min to eliminate air. Flow rate of all carrier gases are kept at 8sccm. Cyclic voltammetry (CV) in the double-layer capacitance region was then scanned multiple times until the curved overlapped. This was done to reduce the catalyst surface area. Electrochemistry was controlled using a BioLogic Sp-200 potentiostat. Unless otherwise stated, the working electrode potential (E_{WE}) was recorded and referenced against the mercury sulfate reference electrode and converted to the SHE or RHE scale according to:

$$E_{SHE} = E_{WE} + E_{RE} \qquad (1)$$

$$E_{RHE} = E_{WE} + E_{RE} + 0.059 * pH \qquad (2)$$

where, E_{RE} is 0.644V vs. SHE at 25°C.

Electrochemical active surface area (ECSA) calculation

The ECSA on Au for ECO_2R was carried out *in situ* by scanning the CV curves from 0.55V to 0.85V vs. RHE at various rates (10, 20, 30, 40, 50 mV/s, respectively). The double layer charging current at 0.70V vs. RHE was then plotted with respect to the scan rate. The double layer capacity is given by:

$$i = \frac{dQ}{dt} = \frac{dQ}{dE} * \frac{dE}{dC} = C * v \qquad (3)$$

where, *C* is capacitance (F/cm^2), and *v* is the scan rate (mV/s).

ECSA was calculated by referring the obtained capacity to the reference value C_{ref} (210mF/cm^2) (previously calculated on the same electrode after mechanical polishing, electro-polishing and flame annealing, data not shown here). ECSA calculation was performed after each run of electrochemistry.

Data processing

Quantification of the electrochemical mass spectrometry data was determined by the sensitivity factor (F_M^i) for each analyte *i* at a suitable mass-to-charge ratio (*m/z*), at which the signal is an exclusive indicator of the desired analyte, or at least the interference of the others is negligible or easily differentiable. For example, the corresponding m/z of H_2, He, CH_4, C_2H_4, and CO_2 was set to be 2, 4, 15, 26, and 44, respectively. Although m/z 28 is usually a combination of N_2 and CO signals, the contribution from N_2 is usually over two orders of magnitude lower

than CO under reaction conditions and is therefore negligible. Alternatively, it could also be easily extracted by normalizing with the background before electrochemical measurements. In addition, CO_2 also produces CO^+ fragments from self-dissociation during ionization and thus complicates the quantitation of CO production in ECO_2R. This issue can be properly addressed using selective ionization, which will be described in detail in Section 3.3.

The molar flow rate of an analyte *i* going from the electrochemical cell to the QMS ($\dot{n}_i$) is in a linear relationship with the QMS signal (S_M^i) by the factor of ($1/F_M^i$):

$$\dot{n}_i = \frac{S_M^i}{F_M^i} \tag{4}$$

According to Faraday's law, the Faradaic efficiency of a product is given by:

$$FE_i = \frac{zF\dot{n}_i}{I_T t} \tag{5}$$

where, *z* is the number of transferred electrons for producing *i*, *F* is the Faraday's constant (96485 C/mol), I_T is the total current of the reaction, and *t* is the reaction time.

It is noteworthy that F_M^i of a certain analyte will be constant for the same membrane chip (**Error! Reference source not found.**) when the reactions happen in the same atmospheric environment (i.e. temperature, pressure, and carrier gas flow rate), which has been kept the same for all measurements shown in the current report. In principle, F_M^i of each analyte should be calibrated in order to quantitatively link S_M^i and the corresponding $\dot{n}_i$, following the process described by [20]. Unfortunately, due to technical issues, calibration has not been done yet, but a qualitative comparison among products going through the same membrane chip is possible. For example, in the case of ECO_2R on Au, the only detected gaseous products are Co and H_2. To compare the selectivity between them, the following principle can be used:

$$\frac{FE_{CO}}{FE_{H_2}} = \frac{\frac{z_{CO}F\dot{n}_{CO}}{I_T t}}{\frac{z_{H_2}F\dot{n}_{H_2}}{I_T t}} = \frac{\frac{z_{CO}F}{I_T t} * \frac{S_{28}^{co}}{F_{28}^{co}}}{\frac{z_{H_2}F}{I_T t} * \frac{S_2^{H_2}}{F_2^{H_2}}} = \left(\frac{\frac{z_{CO}F}{I_T t}}{\frac{z_{H_2}F}{I_T t}}\right) * \left(\frac{F_2^{H_2}}{F_{28}^{co}}\right) * \left(\frac{S_{28}^{co}}{S_2^{H_2}}\right) \tag{6}$$

where, $z_{CO} = z_{H_2} = 2$; F, I_T, and t are all constants in the same measurement, while $\left(\frac{F_2^{H_2}}{F_{28}^{co}}\right)$ is also a constant on the same chip. The above equation then gives:

$$\frac{FE_{CO}}{FE_{H_2}} \propto \left(\frac{S_{28}^{co}}{S_2^{H_2}}\right) \tag{7}$$

Also, partial current density j_i can be written as:

$$j_i = j_T * FE_i = \left(\frac{I_T}{A}\right) * \left(\frac{zF}{I_T t}\right) * \left(\frac{S_M^i}{F_M^i}\right) = \left(\frac{zF}{A t F_M^i}\right) * S_M^i \tag{8}$$

$$j_i \propto S_M^i \tag{9}$$

Therefore, the activity and selectivity can be compared by directly comparing the QMS signal when measurements are conducted on the same chip and under the same atmospheric environment.

3.2 Electrochemical CO and CO₂ Reduction on Copper

Electrochemical CO_2 reduction on Cu was performed by chronoamperometry in CO_2-saturated 0.1M $KHCO_3$ (pH ~6.8), during which CO_2 was used as the carrier gas and was kept purged throughout the measurement. The applied potential was stepped down every 50mV and kept at each value for 5min. The results are depicted in Figure 1a. The peak/valley appeared at ~3800s was due to an accidently jumped E_{WE}, which does not seem to have a significant influence on the following measurement. Hydrogen evolution reaction (HER) onset at -0.15V vs. RHE, illustrating the high sensitivity of the experimental setup. From the plot it is obvious that HER predominated during the entire experiment course. Water has been proven to be the major proton donor under ECO_2R conditions, following Equation (10) [21], [22]. The produced OH^- led to an increased local pH at the electrode surface, which consumed CO_2 (Equation (11)) [1], [23]–[25] and therefore a reduced m/z 44 (CO_2) signal was exhibited in the plot. The m/z 28 was mainly from the CO^+ fragment due to CO_2 dissociation as explained before, and thus decreased as well. The C_2H_4 (m/z 26) onset at -0.50V vs. RHE, but only had a faint increment and did not increase further until the end of the measurement. It was because when the E_{WE} exceeded -0.55 V vs. RHE, not only did the reaction become mass transfer limited, but as H_2 was continuously produced, the non-dissolved H_2 would build up a large amount of bubbles in the system, preventing electrons from transferring between the working and the counter electrode, and the potentiostat would control amplifier overloaded (i.e. insufficient voltage) as a result.
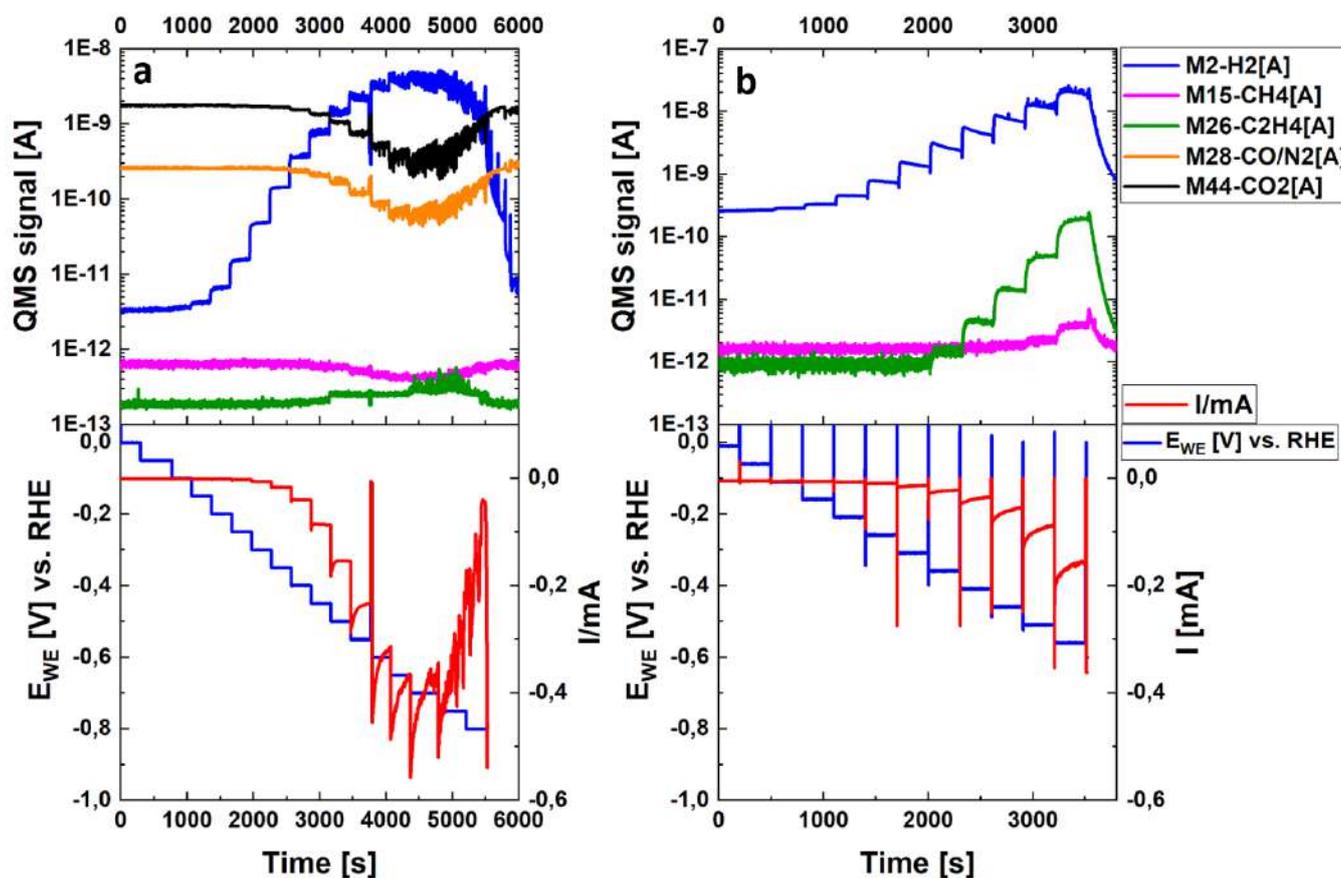
$$2H_2O + 2e^- \leftrightarrow H_2 + 2OH^- \tag{10}$$

$$CO_2 + OH^- \leftrightarrow HCO_3^- \tag{11}$$

Figure 1: Electrochemistry on Cu. Upper panel: direct quadrupole mass spectrometer signal; bottom panel: applied potential (left axis) and total current (right axis). a) Electrochemical CO_2 reduction performed on polycrystalline Cu electrode in CO_2-

saturated 0.1M KHCO$_3$ (pH ~6.8) electrolyte; b) Electrochemical CO reduction performed on polycrystalline Cu electrode in CO-saturated 0.1M K$_2$CO$_3$ (pH ~11.5) electrolyte.

The bubble-induced overloading problem is inevitable when a large number of bubbles are produced, which is a technical limitation of the EC-MS system. Thus we have discovered this is a fundamental limitation towards our quest to investigate the ethano/ethylene branching ratio. However, one way to avert this issue is to do ECOR in 0.1M K$_2$CO$_3$ (pH 11.5) instead. Since HER is more favorable in acidic electrolytes, and *CO competes for the same adsorption sites with *H [26], hydrogen production and thus bubble creation could be restrained. More importantly, CO has been widely accepted as the first and most crucial intermediate of ECO$_2$R to produce C$_{2+}$ products, as it has the same product distribution as ECO$_2$R and simplifies the buffer impacts of electrolytes [1], [22], [26].

As depicted in Figure 1b, HER and ECOR onset at -0.12 v and -0.37V vs. RHE, respectively. C$_2$H$_4$ signal increase was much more pronounced compared to in the case of ECO$_2$R. CH$_4$ onset at -0.52V vs. RHE was also noticeable. On the other hand, the potentiostat was overloaded again when E$_{WE}$ exceeded -0.60V vs. RHE due to the produced gas bubbles in the system, which further manifests the high sensitivity yet low bubble resistance of the EC-MS setup.

Throughout this work ethanol was not detected. It should be noted though that other experiments doen in our lab using polycrystalline Cu has shown in ethanol (See deliverable 3.1), thus it is believed that the low vapor pressure, and concomitant lack of sensitivity for the Sniffer chip is the reason for not being able to see this in the mass spectrometer.

3.3 Electrochemical CO$_2$ Reduction on Gold_Selective Ionization
ECO$_2$R on Au was carried out to investigate CO production, which will provide informative mechanistic insights for building up Cu-Au tandem catalysts in the future.

As mentioned before, the intensity variation of the m/z 28 signal follows that of m/z 44 due to CO$_2$ fragmentation. Since the appearance energy of CO$_2$ dissociation to CO$^+$ is relatively low (~20eV, NIST [27]) compared to the employed MS ionization energy (normally 70 V), m/z 28 signal usually has a high background level when the system is purged with CO$_2$, as illustrated in Figure 1a. In order to alleviate the CO$^+$ contribution in the m/z 28 signal, Bondue and Koper reduced the ion source energy from 70 V to 27.5 V using Differential Electrochemical Mass Spectrometry (DEMS) and realized a direct detection of CO formed during ECO$_2$R. As can be seen in Figure 2a, there is an obvious increment of I_Ion(28) in the oxygen evolution reaction (OER) region, which was too anodic for "real" CO to exist; while in the HER region, where CO was supposed to be produced and give an increased signal, it reduced following the dropped CO$_2$ signal instead. This was attributed to the overwhelming contribution of CO$_2$ fragmentation over the "real" CO in the m/z 28 signal. As the ionization energy was reduced to 27.5V, I_Ion(28) reflected the real CO amount. [28]
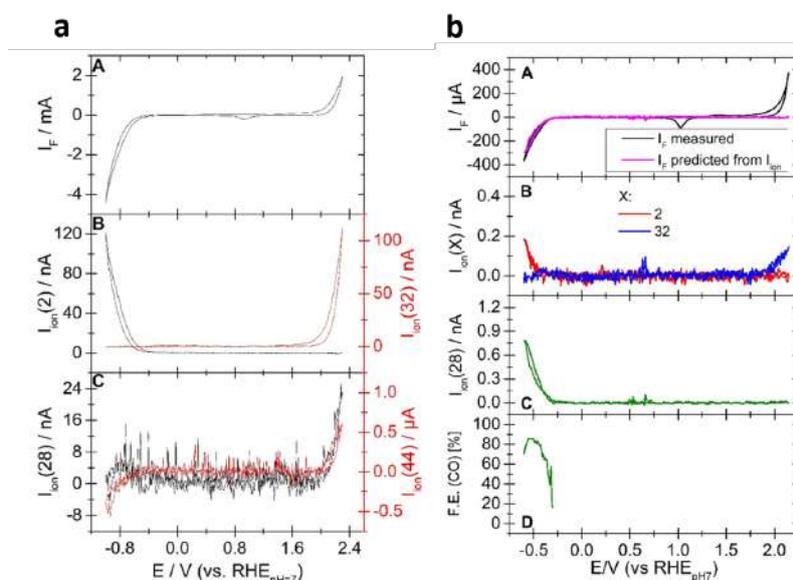
Figure 2: Comparison of DEMS experiment results acquired on different cathode potential of ion source. a) The working electrode is a thin gold film (approximately 50 nm) sputter deposited on the Teflon membrane. The electrolyte is an aqueous solution of 0.9 M $NaClO_4$ and 0.1 M $NaHCO_3$ purged with CO_2. A: faradaic current; B: Ionic current for mass 2 (black curve, left y-scale) and for mass 32 (red curve, right y-scale); C: Ionic current for mass 28 (black curve, left y-scale) and for mass 44 (red curve, right y-scale). Cathode potential of ion source: −70 V. Sweep rate: 20 mV/s. b) The working electrode is a massive, polycrystalline gold. The electrolyte is an aqueous solution of 0.9 M $NaClO_4$ and 0.1 M $NaHCO_3$ purged with CO_2. A: measured faradaic current (black) and faradaic current determined from the ionic current for mass 2 and 28 (magenta); B: Ionic current for mass 2 (red) and mass 32 (blue); C: Ionic current for mass 28. D: Faradaic efficiency for CO formation as determined from the ionic current for mass 2 and 28. Cathode potential of ion source: −27.5 V. Sweep rate: 20 mV/s. Reprinted from Bondue et al. [28]

Inspired by their work, we reduced our QMS ionization energy from 70eV to 23eV. The m/z 28 signal was reduced over one order of magnitude (Figure S3), while the m/z 44 background stayed at the same level.

ECO_2R measurements on Au were subsequently performed with selective ionization under the same reaction conditions as on Cu. Initially the pristine Au electrode was tested (Figure 3a). Due to the bubble issues described before, the potentiostat overloaded at EWE -0.45V vs. RHE. Only HER was detected within this potential limitation. CO_2 consumption was assigned to the homogenous equilibrium reactions due to the HER-induced increasing local pH.

Previous studies have shown both exerimentally and theoretically that undercoordinated sites on the Au surface are more active for CO production than HER [4], [8], [29]–[33]. For example, DFT calculations carried out by Back et al. suggested that corner sites were the most active for CO_2 reduction to CO, while edge sites favoured both CO and H_2 production under ECO_2R conditions [4]. By contrast, experimental results combining electron backscatter diffraction (EBSD) and scanning electrochemical cell microscopy (SECCM) revealed that unlike ECO_2R, HER does not depend on undercoordinated sites in a slightly acidic sodium citrate electrolyte (10mM, pH 5.5) [29]. Another study compared the simulation and experimental results of Au catalysts with various facets for ECO_2R under a near-neutral condition (0.1M KHCO3, pH 6.8), and disclosed a similar trend: while CO_2R to CO exhibited a strong dependence on facet, HER was similar for all tested catalysts irrespective to their surface structure [8].
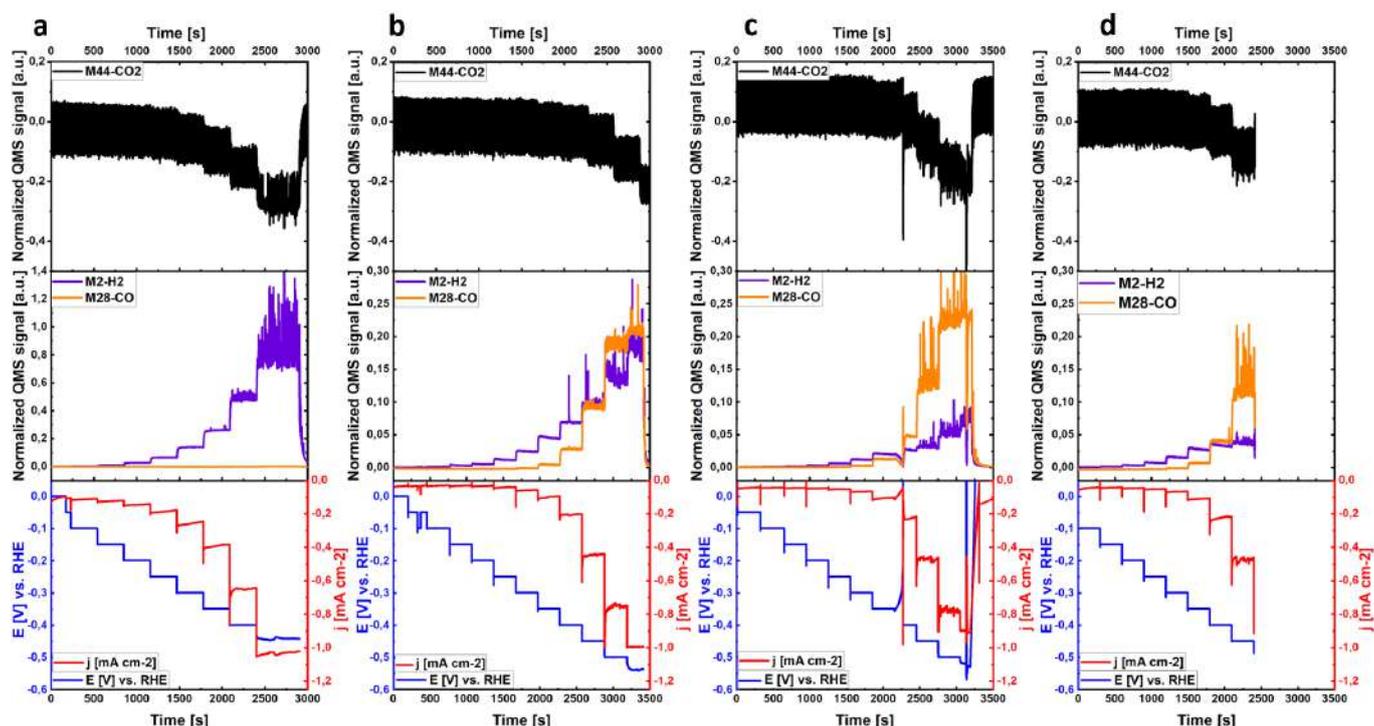
Figure 3: Electrochemical CO₂ reduction on Au in CO₂-saturated 0.1M KHCO₃ electrolyte (pH ~6.8), using the same electrode but with different surface roughness, normalized by geometric surface area. a) Pristin (flat) Au surface; b) R1 Au surface, roughened in situ for 1h; c) R2 Au surface_1st run, roughened in situ for 2h; d) R2 Au surface_2nd run, performed after the 1st run, the electrolyte was refreshed without removing or remounting the cell, electrochemistry was triggered after all signals dropped back to their baselines. QMS signals are normalized by first extracting each of their own background signals before the electrochemistry, then divided by the CO₂ background signal (the highest) to eliminate influences of the electron multiplier on the signal intensity.

Based on the above evidence, we expected a promoted CO generation on a roughened Au surface. Surface roughening was performed in situ following the description in the "Electrode Preparation" session for 1h (noted as R1) and 2h (noted as R2), respectively. The electrochemical data and QMS signals are first normalized by geometric surface area shown in Figure 3 to give a preliminary evaluation of the roughening effects. It can be seen that as the electrode surface was roughened, HER was significantly suppressed while CO was remarkably improved. This seems to be contradictory to previous findings that HER did not greatly depend on the surface roughness. Furthermore, total current densities also dropped on rougher Au surfaces compared to the pristine one. One possibility is that previous studies were usually performed before mass transfer limitation occurs such that the acquired activity was more likely to be intrinsic. Our system, however, is a batch reactor with a relatively small reaction volume and thus is more likely to be mass transfer limited. Moreover, considering that H_2O and CO_2 compete for the same adsorption sites on Au under ECO₂R conditions with the activation of CO_2 being energetically preferred [8], it is possible that the produced CO poisoned the roughened Au surface, preventing H_2O adsorption and hence inhibited HER, which in turn weakened the local alkalinity and further enhanced CO production, as shown in Equation 11. However if we do have bound CO to the Au, the idea of a mixed Au/Cu catalyst does have potential if the CO can migrate from the Au to the Cu. This different way of binding to CO could potentially allow us to get different ethylene/ethanol ratios and along with computational modeling and other experiments help understand the branching of the ethanol/ethylene branching ratio. However the electric field may also contribute to the facilitated CO₂R. A recent study has revealed that tips of Au needles produced local high electric fields that concentrated K⁺, which in turn led

to a high local CO_2 adsorption close to the active CO_2R sites. Simulations further confirmed that the adsorbed K^+ could lower the thermodynamic energy barrier for CO_2 to CO conversion [34].

$$CO_2 + 2e^- \leftrightarrow CO + OH^-$$

(12)

Another possible reason for the distinct HER suppression is that the applied potentials in previous studies are usually below -0.6V vs. RHE, which is more negative than ours. Overpotentials may influence the reaction mechanism of HER and CO_2R respectively and the interplay between them as well. For instance, Ringe et al.'s recent theoretical study proposed a model that reveals the RDS of CO_2R to CO to be *COOH to *CO at low overpotentials, CO_2 adsorption at intermediate ones, and CO_2 mass transport at high overpotentials [35]. Chen et al. also proposed different mechanisms for CO_2R to CO on polycrystalline Au and oxide-derived Au based on Tafel analysis, for which the RDS in the former was the initial e^- transfer to CO_2 to form an adsorbed $CO_2^{\bullet-}$ intermediate, while in the latter was H^+ transfer with HCO_3^- serving as the H^+ donor [32]. Kinetic studies would provide more insights on the influence of overpotentials, which is in the future plan.

The higher current density baseline in the pristine Au measurement might be owing to that the Au electrode was not completely reduced after flame annealing in air. ECSA-normalized data could certainly provide more insights on the reaction mechanism and kinetics. However, due to technical issues the measurement results were not reliable (Figure S4). Future works will be based on ECSA-normalized analysis.

To examine the stability of the roughened surface, the R2 sample was tested for two consecutive runs. Specifically, after the first run, the electrolyte was refreshed without dismounting the cell, and waited until all signals went back to their baselines. The reproducibility kept well until EWE reached -0.5V vs. RHE at which point the potentiostat overloaded again.

3.4 KHCO₃ Dissociation on Au under Electrochemical CO₂ Reduction conditions

As mentioned before, homogenous equilibrium reactions among the buffer species in the electrolyte play an important role in ECO_2R. To further verify this, $KHCO_3$ dissociation was performed in the absence of an external CO_2 supply. The measurement was conducted in an Ar saturated-0.5M $KHCO_3$ electrolyte (pH~8.4) that ensured a large amount of HCO_3^- anions.
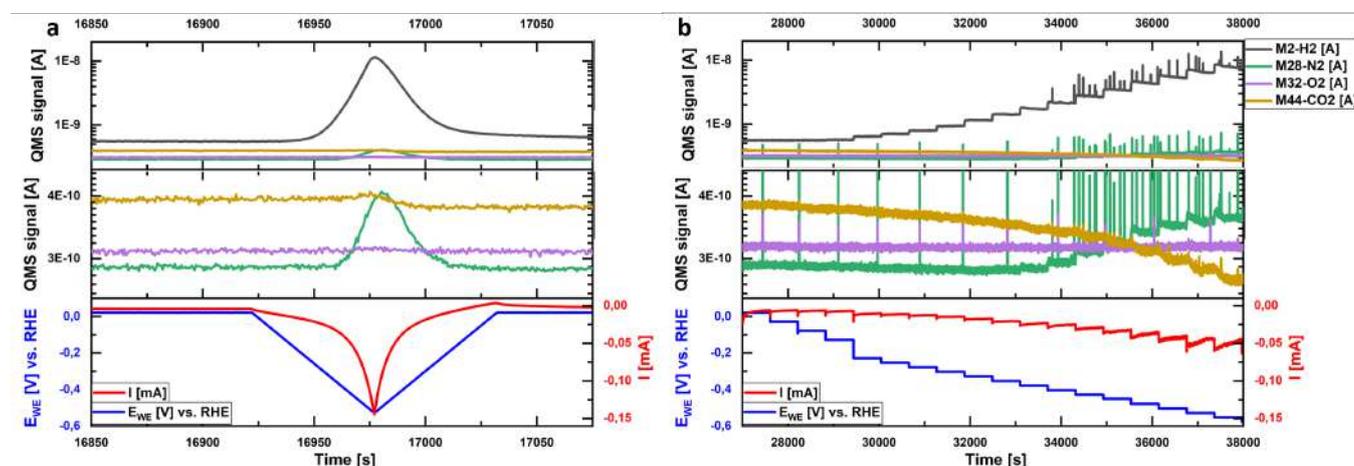

Figure 4 Electrochemical CO₂ reduction on Au performed in Ar-saturated 0.1M KHCO₃ electrolyte (pH ~8.4). a) Cyclic voltammetry carried out between 0 to -0.55V vs. RHE, scan rate 10mV/s. b) Chronoamperometry carried out between 0 to -0.55V vs. RHE. The potential was stepped down every 50mV and kept at each value for 5min. Periodic

SELECTCO2 Deliverable Report D.3.2 – Report on Sniffer Chip discoveries relating to ethanol/ethylene branching mechanism - 28/05/2021 – Version 1.0

13

spikes are due to the created bubbles in the system, which does not seem to have a noticeable influence on the measurement itself.

The enlarged cyclic voltammetry (Figure 4a) exhibited a pronounced CO signal (m/z 28) increase in the cathodic region, where a slight decrease in the CO_2 signal (m/z 44) was also noticeable. Chronoamperometry studies (Figure 4b) verified the same phenomena. Considering that HCO_3^- was the only carbon source in the system, both CO and CO_2 were undoubtedly from HCO_3^- either directly or indirectly. Specifically, CO_2 was from the self-dissociation of HCO_3^- following Equation 13, which was further reduced to CO under cationic potentials. It is noteworthy that selective ionization was not applied to this measurement since the CO background would be so low that it would be out of the detection limit. Moreover, as the CO_2 signal decreased, the contribution of its fragmentation to the increased CO signal is negligible. The periodic spicks are bubbles created in the system as explained before.

$$HCO_3^- \leftrightarrow CO_2 + OH^-$$

(13)

4. CONCLUSIONS AND FUTURE WORK

The object of WP3 is to promote the Faradaic efficiency of ethanol by taking advantage of the synergistic interaction between Cu and Au/Ag. As an initial stage, we investigated the ECO_2R performance on pure Cu and Au electrodes separately.

Early onset of C_2 products on polycrystalline Cu electrode at -0.50V and -0.37V vs. RHE were presented for ECO_2R and ECOR, respectively. CH_4 production was also observed from -0.52V vs. RHE in ECOR. In the future we will perform the same measurements on Cu single crystals including (100), (110), (111), and (211) facets and obtain more fundamental understandings on the reaction mechanisms. Previous efforts on special holder for mounting single crystal electrodes into the cell will be briefly presented in Appendix A6.

Selective ionization on Au for ECO_2R successfully mitigated CO_2 fragmentation and provided more explicit information on CO_2 reduction to CO. Roughening of the Au electrode surface was realized by in situ cycling between strongly anodic and cathodic potentials, leading to a significantly suppressed HER while evidently promoted CO production. It was preliminarily explained as the result of an increased local pH and a stronger electric field. Besides, overpotential and faceting could also have impacts on the reaction mechanism. More efforts will be put on mechanistic studies in the future. Furthermore, the current results are mostly qualitative evaluations based on the geometric surface area. More deliberated quantitative analysis based on the electrochemical active surface area will be performed in the future.

CO produced in an Ar-saturated $KHCO_3$ electrolyte under ECO_2R conditions confirmed that CO_2 could be generated "internally" from homogenous equilibrium reactions of buffering species in the electrolyte. This will help elucidate the influence of local pH on ECO_2R. This is essential because recent literature has shown an increased pH leads to more acetate at the expense primarily of ethanol, but also of ethylene [36]. If we can use this method to provide an accurate local pH and precise ethylene concentrations, further ex-situ liquid product analysis along with mass transfer and DFT modeling should allow us to gain significant insight into this branching . The influence of the electrode surface roughness and overpotentials on the reaction mechanism will give us additional tools on which we will focus on in the future.

In addition to investigating more on Cu and Au separately, future works will pay more attention to linking their interaction with the bifurcation between C_2H_4 and EtOH production. Bimetallic catalysts of Cu and Au will be prepared with potentially different interfaces prepared using various methods, such as sputtering, lithography electro-deposition, and galvanic exchange. Furthermore we also intend to introduce isotope labelled species to better help us understand this reaction. Due to supply chain issues (we believe Covid-1+ related) we were not able to obtain this for this deliverable.

The employed EC-MS setup enabled a real-time detection of the generated gas products. With the high time and mass resolution, it realized high sensitivity and fast time response to gas molecules with a 100% collection efficiency. On the other hand, the high sensitivity and small reaction volume also incur bubble issues and therefore limit more negative overpotentials to be applied. Furthermore, as previously mentioned, the EC-MS system is not optimally suitable to detect liquid products. Thus, future works regarding liquid products will also include work related to H-type cell devices.

This deliverable show that the Sniffer device approach has limited capabilities to elucidate the ethylene to ethanol branching mechanisms in itself. However it does provide highly unique information, such as excellent detection of products, reactions with homogenously evolved species (such as CO_2 from bicarbonate) and variations due to surface roughness. Thus the overall conclusion is that results from the Sniffer device will need to work in conjunction with other techniques to fully help resolve the branching mechanism between ethylene and ethanol.

It should be noted that the SELECTCO2 proposal for applying for synchrotron beamlines at SSRL has been accepted and we expect to have time somewhere between Ocotber-March. This work will focus on in situ and operando studies of bimetallic CuAg catalysts for ECO_2R and ECOR for the bifurcation between ethylene and ethanol production. While the present deliverable has given us some thoughts on the optimal issues to investigate, the future work on the Sniffer chip preceeding that will let us refine what to study during the beamtime. Furthermore, we will take results from the beamtime and iteratively use these again to design new Sniffer Chips and H-Cell experiments to further investigate the ethanol/ethylene branching ratio.

5. REFERENCES

[1]   S. Nitopi *et al.*, "Progress and Perspectives of Electrochemical CO2 Reduction on Copper in Aqueous Electrolyte," *Chem. Rev.*, vol. 119, no. 12, pp. 7610–7672, 2019, doi: 10.1021/acs.chemrev.8b00705.

[2]   H. Jia *et al.*, "Symmetry-Broken Au–Cu Heterostructures and their Tandem Catalysis Process in Electrochemical CO2 Reduction," *Adv. Funct. Mater.*, vol. 2101255, pp. 1–11, 2021, doi: 10.1002/adfm.202101255.

[3]   T. J. Haynes, W. M., Lide, D. R., & Bruno, *CRC handbook of chemistry and physics: a ready-reference book of chemical and physical data*, 97th ed. Florida: CRC Press, 2016.

[4]   S. Back, M. S. Yeom, and Y. Jung, "Active Sites of Au and Ag Nanoparticle Catalysts for CO2 Electroreduction to CO," *ACS Catal.*, vol. 5, no. 9, pp. 5089–5096, 2015, doi: 10.1021/acscatal.5b00462.

[5]   C. G. Morales-Guio *et al.*, "Improved CO2 reduction activity towards C2+ alcohols on a tandem gold on copper electrocatalyst," *Nat. Catal.*, vol. 1, no. 10, pp. 764–771, 2018, doi: 10.1038/s41929-018-0139-9.

[6]   Y. Lum and J. W. Ager, "Sequential catalysis controls selectivity in electrochemical CO2 reduction on Cu," *Energy Environ. Sci.*, vol. 11, no. 10, pp. 2935–2944, 2018, doi: 10.1039/c8ee01501e.

[7]   J. Gao, D. Ren, X. Guo, S. M. Zakeeruddin, and M. Grätzel, "Sequential catalysis enables enhanced C-C coupling towards multi-carbon alkenes and alcohols in carbon dioxide reduction: A study on bifunctional Cu/Au electrocatalysts," *Faraday Discuss.*, vol. 215, pp. 282–296, 2019, doi: 10.1039/c8fd00219c.

[8]   S. Mezzavilla, S. Horch, I. E. L. Stephens, B. Seger, and I. Chorkendorff, "Structure Sensitivity in the Electrocatalytic Reduction of CO 2 with Gold Catalysts," *Angew. Chemie - Int. Ed.*, vol. 58, no. 12, pp. 3774–3778, 2019, doi: 10.1002/anie.201811422.

[9]   Y. C. Li *et al.*, "Binding Site Diversity Promotes CO2 Electroreduction to Ethanol," *J. Am. Chem. Soc.*, vol. 141, no. 21, pp. 8584–8591, 2019, doi: 10.1021/jacs.9b02945.

[10]   X. Zhi, Y. Jiao, Y. Zheng, A. Vasileff, and S. Z. Qiao, "Selectivity roadmap for electrochemical CO2 reduction on copper-based alloy catalysts," *Nano Energy*, vol. 71, no. October 2019, p. 104601, 2020, doi: 10.1016/j.nanoen.2020.104601.

[11]   S. Shen *et al.*, "AuCu Alloy Nanoparticle Embedded Cu Submicrocone Arrays for Selective Conversion of CO2 to Ethanol," *Small*, vol. 15, no. 37, pp. 1–7, 2019, doi: 10.1002/smll.201902229.

[12]   F. Jia, X. Yu, and L. Zhang, "Enhanced selectivity for the electrochemical reduction of CO2 to alcohols in aqueous solution with nanostructured Cu-Au alloy as catalyst," *J. Power Sources*, vol. 252, pp. 85–89, 2014, doi: 10.1016/j.jpowsour.2013.12.002.

[13]   B. Hammer and J. K. Nørskov, "Electronic factors determining the reactivity of metal surfaces," *Surf. Sci.*, vol. 343, no. 3, pp. 211–220, 1995, doi: 10.1016/0039-6028(96)80007-0.

[14]   K. Liu *et al.*, "Electronic Effects Determine the Selectivity of Planar Au-Cu Bimetallic Thin Films for Electrochemical CO 2 Reduction," *ACS Appl. Mater. Interfaces*, vol. 11, no. 18, pp. 16546–16555, 2019, doi: 10.1021/acsami.9b01553.

[15]   J. H. Kim *et al.*, "Highly active and selective Au thin layer on Cu polycrystalline surface prepared by galvanic displacement for the electrochemical reduction of CO2 to CO," *Appl. Catal. B Environ.*, vol. 213, pp. 211–215, 2017, doi: 10.1016/j.apcatb.2017.05.001.

[16]   X. Kong, C. Wang, H. Zheng, Z. Geng, J. Bao, and J. Zeng, "Enhance the activity of multi-carbon products for Cu via P doping towards CO2 reduction," *Sci. China Chem.*, 2021, doi: 10.1007/s11426-020-9934-0.

[17]   D. B. Trimarco *et al.*, "Enabling real-time detection of electrochemical desorption phenomena with sub-monolayer sensitivity," *Electrochim. Acta*, vol. 268, pp. 520–530, 2018, doi: 10.1016/j.electacta.2018.02.060.

[18]   J. H. Baricuatro, Y. G. Kim, C. L. Korzeniewski, and M. P. Soriaga, "Tracking the prelude of the electroreduction of carbon monoxide via its interaction with Cu(100): Studies by operando scanning tunneling microscopy and infrared spectroscopy," *Catal. Today*, no. March 2019, pp. 0–1, 2020, doi: 10.1016/j.cattod.2020.01.028.

[19]   E. L. Clark, C. Hahn, T. F. Jaramillo, and A. T. Bell, "Electrochemical CO2 Reduction over Compressively Strained CuAg Surface Alloys with Enhanced Multi-Carbon Oxygenate Selectivity," *J. Am. Chem. Soc.*, vol. 139, no. 44, pp. 15848–15857, 2017, doi: 10.1021/jacs.7b08607.

[20]   S. B. Scott, "Isotope-Labeling Studies in Electrocatalysis for Renewable Energy Conversion, and the Net Carbon Impact of this PhD Project," Technical University of Denmark, 2019.

[21]   A. Goyal, G. Marcandalli, V. A. Mints, and M. T. M. Koper, "Competition between CO2Reduction and Hydrogen Evolution on a Gold Electrode under Well-Defined Mass Transport Conditions," *J. Am. Chem. Soc.*, vol. 142, no. 9, pp. 4154–4161, 2020, doi: 10.1021/jacs.9b10061.

[22]   H. Ooka, M. C. Figueiredo, and M. T. M. Koper, "Competition between Hydrogen Evolution and Carbon Dioxide Reduction on Copper Electrodes in Mildly Acidic Media," *Langmuir*, vol. 33, no. 37, pp. 9307–9313, 2017, doi: 10.1021/acs.langmuir.7b00696.

[23]   S. Zhu, B. Jiang, W. Bin Cai, and M. Shao, "Direct Observation on Reaction Intermediates and the Role of Bicarbonate Anions in CO2 Electrochemical Reduction Reaction on Cu Surfaces," *J. Am. Chem. Soc.*, vol. 139, no. 44, pp. 15664–

15667, 2017, doi: 10.1021/jacs.7b10462.

[24] A. S. Varela, M. Kroschel, T. Reier, and P. Strasser, "Controlling the selectivity of CO2 electroreduction on copper: The effect of the electrolyte concentration and the importance of the local pH," *Catal. Today*, vol. 260, pp. 8–13, 2016, doi: 10.1016/j.cattod.2015.06.009.

[25] R. Kortlever, K. H. Tan, Y. Kwon, and M. T. M. Koper, "Electrochemical carbon dioxide and bicarbonate reduction on copper in weakly alkaline media," *J. Solid State Electrochem.*, vol. 17, no. 7, pp. 1843–1849, 2013, doi: 10.1007/s10008-013-2100-9.

[26] A. A. Peterson, F. Abild-Pedersen, F. Studt, J. Rossmeisl, and J. K. Nørskov, "How copper catalyzes the electroreduction of carbon dioxide into hydrocarbon fuels," *Energy Environ. Sci.*, vol. 3, no. 9, pp. 1311–1315, 2010, doi: 10.1039/c0ee00071j.

[27] N. C. Webbook, "Carbon dioxide Electron affinity determinations," 2021. .

[28] C. J. Bondue and M. T. M. Koper, "A DEMS approach for the direct detection of CO formed during electrochemical CO2 reduction," *J. Electroanal. Chem.*, vol. 875, p. 113842, 2020, doi: 10.1016/j.jelechem.2020.113842.

[29] R. G. Mariano *et al.*, "Microstructural origin of locally enhanced CO2 electroreduction activity on gold," *Nat. Mater.*, 2021, doi: 10.1038/s41563-021-00958-9.

[30] M. Liu *et al.*, "Enhanced electrocatalytic CO2 reduction via field-induced reagent concentration," *Nature*, vol. 537, no. 7620, pp. 382–386, 2016, doi: 10.1038/nature19060.

[31] N. Todoroki, H. Tei, H. Tsurumaki, T. Miyakawa, T. Inoue, and T. Wadayama, "Surface Atomic Arrangement Dependence of Electrochemical CO 2 Reduction on Gold: Online Electrochemical Mass Spectrometric Study on Low-Index Au(hkl) Surfaces," *ACS Catal.*, vol. 9, no. 2, pp. 1383–1388, 2019, doi: 10.1021/acscatal.8b04852.

[32] Y. Chen, C. W. Li, and M. W. Kanan, "Aqueous CO2 reduction at very low overpotential on oxide-derived au nanoparticles," *J. Am. Chem. Soc.*, vol. 134, no. 49, pp. 19969–19972, 2012, doi: 10.1021/ja309317u.

[33] R. G. Mariano, K. McKelvey, H. S. White, and M. W. Kanan, "Selective increase in CO2 electroreduction activity at grain-boundary surface terminations," *Science (80-.).*, vol. 358, no. 6367, pp. 1187–1192, 2017, doi: 10.1126/science.aao3691.

[34] M. Liu *et al.*, "Enhanced electrocatalytic CO2 reduction via field-induced reagent concentration," *Nature*, vol. 537, no. 7620, pp. 382–386, 2016, doi: 10.1038/nature19060.

[35] S. Ringe *et al.*, "Double layer charging driven carbon dioxide adsorption limits the rate of electrochemical carbon dioxide reduction on Gold," *Nat. Commun.*, vol. 11, no. 1, 2020, doi: 10.1038/s41467-019-13777-z.

[36] W. Luc *et al.*, "Two-dimensional copper nanosheets for electrochemical reduction of carbon monoxide to acetate," *Nat. Catal.*, vol. 2, no. 5, pp. 423–430, 2019, doi: 10.1038/s41929-019-0269-8.

[37] D. B. Trimarco, "Real-time detection of sub-monolayer desorption phenomena during electrochemical reactions: Instrument development and applications," Technical University of Denmark, 2017.

[38] G. H. Kelsall, N. J. Welham, and M. A. Diaz, "Thermodynamics of ClH2O, BrH2O, IH2O, AuClH2O, AuBrH2O and AuIH2O systems at 298 K," *J. Electroanal. Chem.*, vol. 361, no. 1–2, pp. 13–24, 1993, doi: 10.1016/0022-0728(93)87034-S.
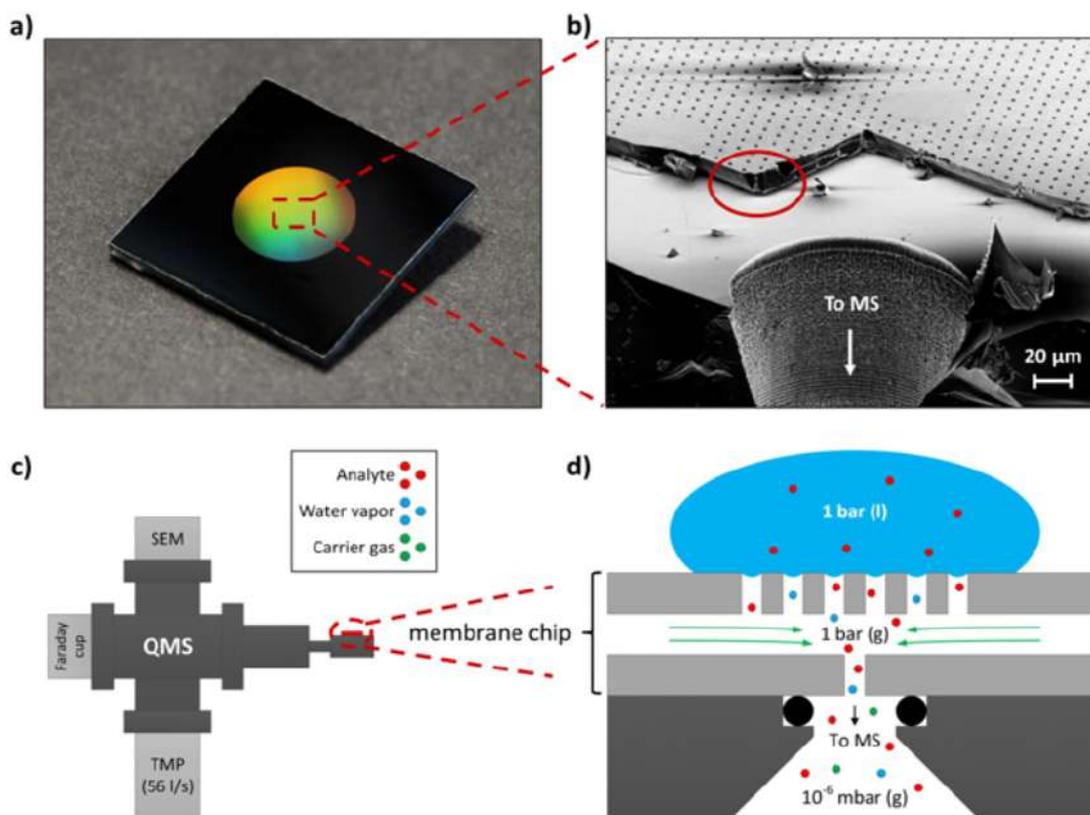
6. APPENDIX

A1 EC-MS SETUP

Figure S1: Membrane chip and working principle. a) Photograph of the membrane chip consisting of a micro porous and hydrophobic membrane suspended across a small internal sampling volume inside the chip. b) Scanning electron microscopy (SEM) image revealing the internal structure of a membrane chip, which has been cut open across the middle of the chip. c) Schematic of the compact mass spectrometer vacuum chamber, to which the membrane chip, here depicted in red, is coupled. d) Schematic illustrating the working principle of the membrane chip, drawn as a schematic side view depiction of the internal structure shown in the SEM image in c. In reality the capillary coupling to UHV is made through a series of capillary channels placed downstream (on the backside of the chip) of the large hole shown in c). Reprinted from [37].

SELECTCO2 Deliverable Report D.3.2 – Report on Sniffer Chip discoveries relating to ethanol/ethylene branching mechanism - 28/05/2021 – Version 1.0

18

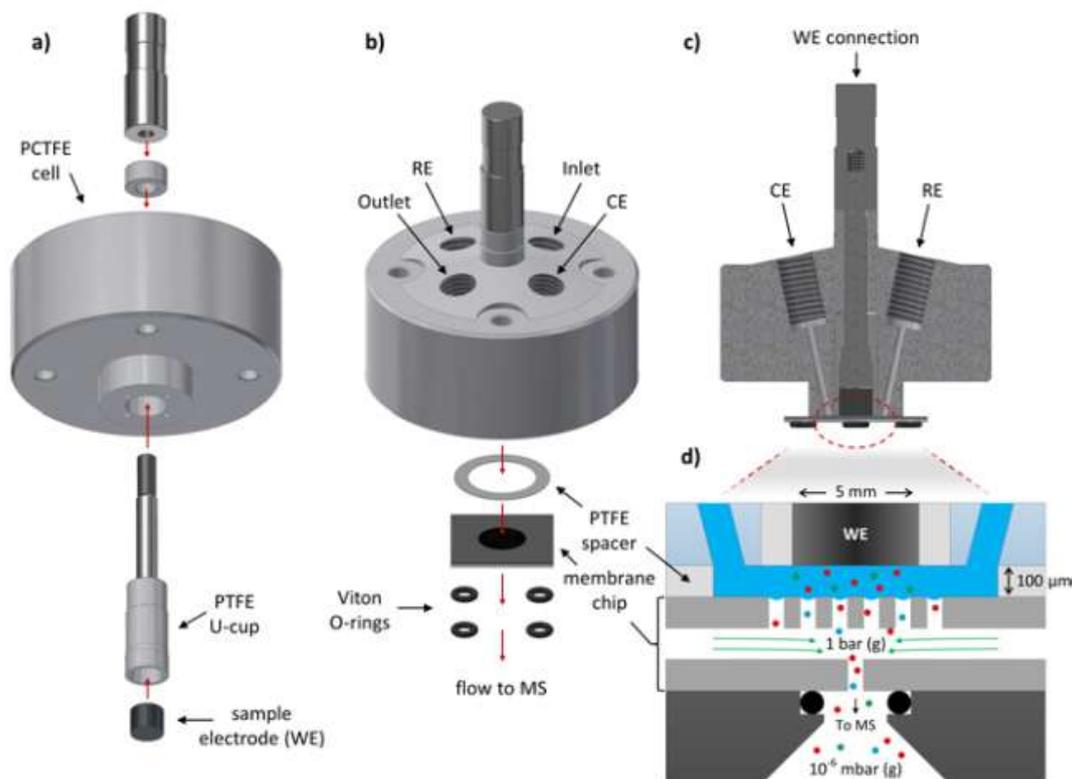## A2 STAGNANT THIN-LAYER CELL

Figure S2: Schematic illustration showing the assembly of the stagnant thin-layer electrochemistry (EC) cell. a) (bottom view) Mounting of a 5.0 mm outer diameter disk electrode in the EC cell using a ChangeDisk RDE electrode mounting system from Pine Resereach Instrumentation. b) (top view) Mounting of the assembled EC cell onto the membrane chip using a 100 µm thick Teflon (PTFE) spacer to define a thin-layer working volume between the electrode and the membrane. Viton O-rings are used to seal the membrane chip to the ultra-high vacuum of the mass spectrometer. Four access channels connect the working volume to an external electrolyte reservoir, a reference electrode (RE) and a counter electrode (CE) using Tefzel (ETFE) Luer adapters (not shown). c) (side cut view) Filling of the EC cell with electrolyte, creating a three electrode configuration established with the working electrode (WE) placed in the center above the membrane. d) (zoomed side view) Working principle showing how volatile reaction products are captured by the membrane and sent to the mass spectrometer while the carrier gas in turn equilibrates with the working volume. The assembled ow cell and the membrane chip interfaces to the mass spectrometer through an interface fange. Reprinted from [37].
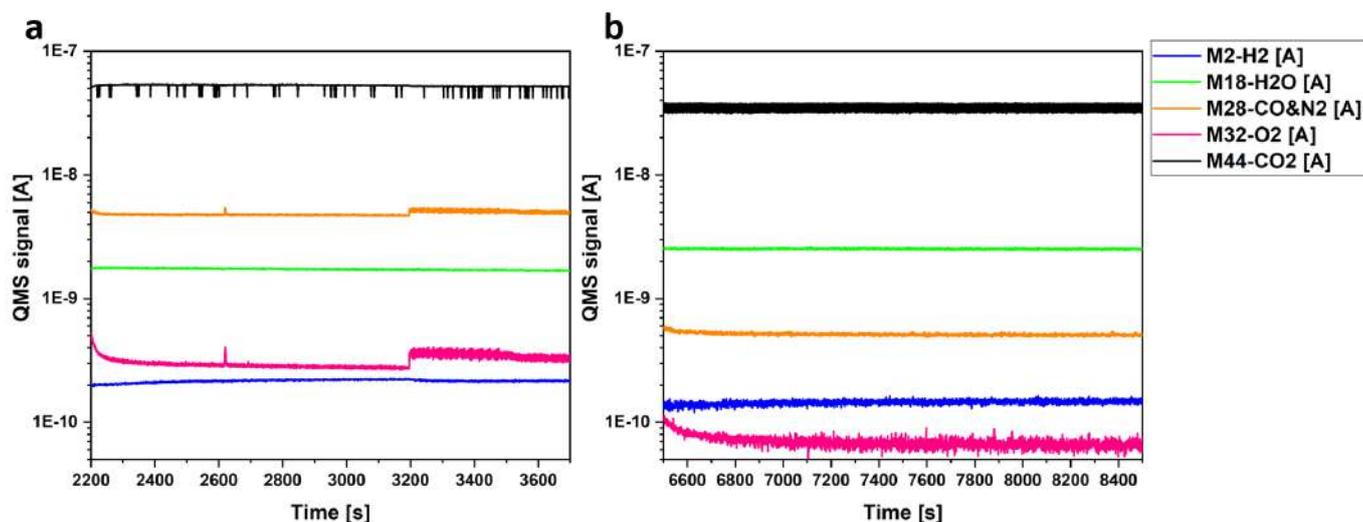
A3 SELECTIVE IONIZATION

Figure S3 Quadrupole mass spectrometer background signal a) with and b) without selective ionsiztaion. Signals were taken with a stagnant thin-layer cell and all three electrodes were mounted and the cell was filled with CO_2-saturated 0.1M $KHCO_3$ electrolyte. CO_2 has been purged at 8sccm for at least 1 hour and waited all signals were stable before each plot was taken. a) Before and b) after

Table 1 Ionizer parameter comparison with and without selective ionization

	Ionizer parameters				
	Emission current (µA)	Electron energy (eV)	Anode potential (V)	Focus potential (V)	Ion energy (meV)
With selective ionization	2000	70	200	27	8000
Without selective ionization	550	23	80	15	8000

SELECTCO2 Deliverable Report D.3.2 – Report on Sniffer Chip discoveries relating to ethanol/ethylene branching mechanism - 28/05/2021 – Version 1.0

20

A4 ECSA-NORMALIZED ELECTROCHEMICAL CO2 REDUCTION ACTIVITY ON GOLD

Table 2 Calculated ECSA on differnet samples

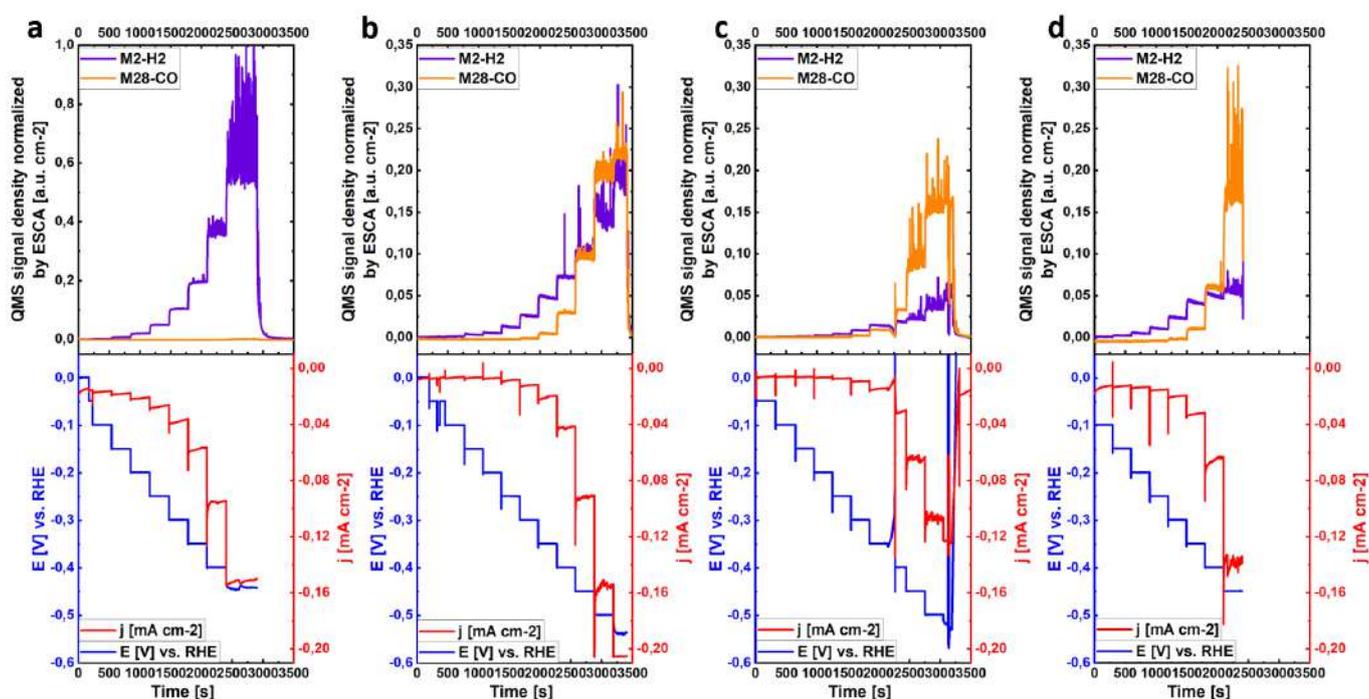| Sample	ECSA (cm^2)
Pristine	1.33
R1	0.95
R2_1st run	1.43
R2_2nd run	0.67

Figure S4: Electrochemical CO$_2$ reduction on Au in CO$_2$-saturated 0.1M KHCO$_3$ electrolyte (pH ~6.8), using the same electrode but with different surface roughness, normalized by electrochemical active surface area. a) Pristin (flat) Au surface; b) R1 Au surface, roughened in situ for 1h; c) R2 Au surface_1st run, roughened in situ for 2h; d) R2 Au surface_2nd run, performed after the 1st run, the electrolyte was refreshed without removing or remounting the cell, electrochemistry was triggered after all signals dropped back to their baselines. QMS signals are normalized by first extracting each of their own background signals before the electrochemistry, then divided by the CO$_2$ background signal (the highest) to eliminate influences of the electron multiplier on the signal intensity.
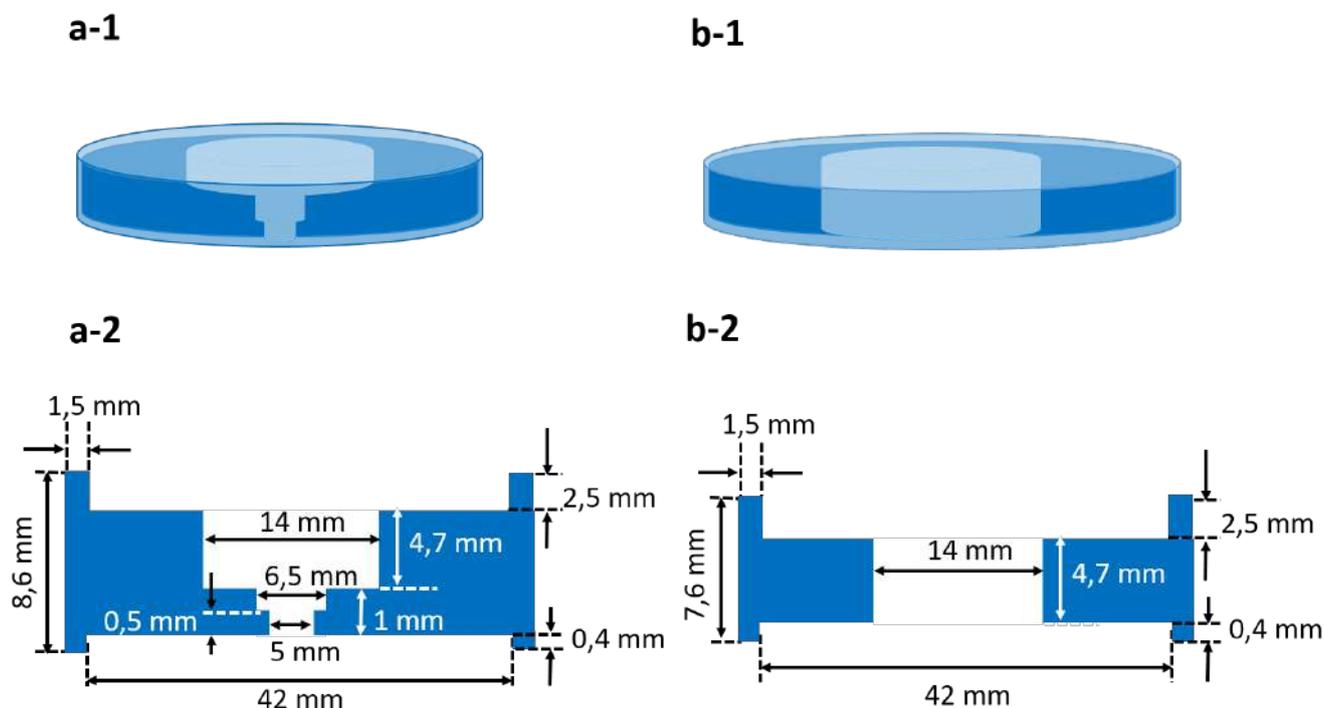
A5 SINGLE CRYSAT HOLDER DESIGN

Figure S5: Single crystal mounting holder design. a-1) Three-dimensional diagram of holder #1, a-2) cross-section of holder #1, b-1) three- dimensional diagram of holder #2, d) cross-section of holder #2. This is a two-step process. Step1. A piece of single crystal silicon wafer (111) will be placed below holder #1, with a piece of lens paper in between, then the Cu single crystal electrode will be placed upside-down (i.e., the surface to be exposed to eæectrochemistry faces down). The electrode will then be placed into the cell following the general procedure with care.Step2. When the electrode is loosely grabbed by the cell, the second holder will be used. The cell holding the holder will be placed on top of holder #2, then slightly push from the top until the electrode is completely pushed into the cell. By this means, the single crystal configuration of the electrode will be protected to the greatest extent.